Journal of Power Sources 186 (2009) 133–137

Contents lists available at ScienceDirect

Journal of Power Sources

journal homepage: www.elsevier.com/locate/jpowsour

Short communication

Bimetallic (Ni–Fe) anode-supported solid oxide fuel cells with gadolinia-doped ceria electrolyte

Hyeon Cheol Park, Anil V. Virkar*

Department of Materials Science and Engineering, 122 S. Central Campus Drive, University of Utah, Salt Lake City, UT 84112, United States

ARTICLE INFO

Article history:
Received 12 August 2008
Received in revised form
17 September 2008
Accepted 20 September 2008
Available online 1 October 2008

Keywords:
Iron–nickel bimetallic anode support
Gadolinia-doped ceria (GDC) electrolyte
Solid oxide fuel cells

ABSTRACT

Anode-supported solid oxide fuel cells (SOFC) comprising nickel + iron anode support and gadolinia-doped ceria (GDC) of composition $Gd_{0.1}Ce_{0.9}O_{2-\delta}$ thin film electrolyte were fabricated, and their performance was evaluated. The ratio of Fe_2O_3 to NiO in the anode support was 3 to 7 on a molar basis. Fe_2O_3 and NiO powders were mixed in the desired proportions and discs were die-pressed. All other layers were sequentially applied on the anode support. The cell structure consisted of five distinct layers: anode support – Ni + Fe; anode functional layer – Ni + GDC; electrolyte – GDC; cathode functional layer – LSC ($La_{0.6}Sr_{0.4}CoO_{3-\delta}$) + GDC; and cathode current collector – LSC. Cells with three different variations of the electrolyte were made: (1) thin GDC electrolyte (~15 μm); (2) thick GDC electrolyte (~25 μm); and (3) tri-layer GDC/thin yttria-stabilized zirconia (YSZ)/GDC electrolyte (~25 μm). Cells were tested with hydrogen as fuel and air as oxidant up to 650 °C. The maximum open circuit voltage measured at 650 °C was ~0.83 V and maximum power density measured was ~0.68 W cm^{-2}. The present work shows that cells with Fe + Ni containing anode support can be successfully made.

1. Introduction

Solid oxide fuel cells (SOFC) are emerging as an important class of power generation devices which can operate on a number of hydrocarbon containing fuels and directly convert chemical energy of oxidation into electricity at a high efficiency [1–3]. Of the various designs of SOFC under development, anode-supported design has been extensively investigated because of the ease of fabrication, ruggedness, and high performance [2,3]. The thickest and structure-supporting component in most anode-supported SOFC is Ni + YSZ. From the standpoint of cost, reducing the thickness of the anode support is desired since nickel and YSZ both are relatively expensive. Currently, some efforts are underway on the development of metal-supported SOFC wherein the supporting component is made of porous stainless steel upon which the cell is formed. For example, Ceres Corporation in UK is developing ceria thin film cells supported on stainless steel substrates with laser-drilled holes [4]. Efforts on the development of YSZ electrolyte cells supported on porous stainless steel tubes are underway at LBL [5]. In both of these cases, the amount of nickel is substantially reduced by the use of stainless steel supports. Recently, Ishihara and co-workers [6] reported on the development of LSGM-based cells with anode containing a mixture of 90% Ni and 10% Fe. The rationale for the use of Fe was to improve anode catalytic activity.

The present work was undertaken with the principal objective of reducing the amount of nickel from the anode support to as low a value as possible and altogether eliminate yttria-stabilized zirconia (YSZ) from the anode support in order to improve the economic viability of SOFC. Iron and nickel are adjacent to each other in the periodic table, and form extensive solid solutions (e.g. α, γ(Fe,Ni)) and intermetallic phases (e.g. $FeNi_3$) [7]. In this research, samples of various compositions containing different amounts of Fe_2O_3 and NiO were fabricated by sintering of powder compacts. The sintered samples were subsequently reduced in 10% H_2 + balance N_2 and ~100% H_2 atmospheres, and their reduction characteristics were investigated. Cells comprising five distinct layers, namely, anode support (Ni + Fe), anode functional layer (Ni + GDC), electrolyte (GDC), cathode functional layer (LSC + GDC), and cathode current collector (LSC) were fabricated. Based on thermo-mechanical properties of the cells, an optimum composition for the anode support was selected for the cell tests. Cells with three electrolyte variations were made: (1) thin GDC electrolyte (~15 μm thickness); (2) thicker GDC electrolyte (~25 μm thickness); and (3) tri-layer electrolyte (GDC–YSZ–GDC of ~25 μm total thickness with 1 μm YSZ). Cell performance was evaluated over a temperature range from 550 °C to 650 °C.

* Corresponding author. Tel.: +1 801 581 5396; fax: +1 801 581 4816.
E-mail address: anil.virkar@m.cc.utah.edu (A.V. Virkar).

0378-7753/$ – see front matter © 2008 Elsevier B.V. All rights reserved.
doi:10.1016/j.jpowsour.2008.09.080

2. Experimental procedure

2.1. Fabrication of Fe_2O_3–NiO samples

The starting materials for the anode support were Fe_2O_3 (Alfa Aesar) and NiO (Atlantic Equipment Engineering). In order to investigate the effect of iron content in the anode support on cell structural integrity and cell performance, three compositions were selected for the initial trials: (1) Fe_2O_3 – 30%, NiO – 70%; (2) Fe_2O_3 – 50%, NiO – 50%; and (3) Fe_2O_3 – 70%, NiO – 30% (all compositions in mol.%). Powders were mixed and ball milled. Bar-shaped samples of approximate dimensions: width ~12.7 mm, thickness ~2.3 mm, and length ~55 mm (in the as pressed state) were fabricated. Samples were sintered in air at 1400 °C for 2 h. X-ray diffraction (XRD) traces of the samples were obtained using Phillips X'Pert Diffractometer with Cu Kα radiation. The sintered samples were then reduced in two reducing atmospheres; ~10% H_2 + balance N_2 and ~100% H_2 at 800 °C for 1 h. For each sample, dimensions before sintering, after sintering, and after reduction in H_2 containing atmospheres were measured. The porosities of the samples were measured (using Archimedes method in accordance with ASTM Standard C 20-00) after reduction in ~100% H_2.

2.2. Fabrication of cells

The anode support composition selected was Fe_2O_3 – 30% and NiO – 70%. This selection was based on structural integrity, as cells made of the other two anode support compositions exhibited delamination and cracking during cell tests. Disc-shaped samples of dimensions ~3.3 cm diameter and ~0.15 cm thickness were formed by die-pressing. The pressed discs were fired at 650 °C for 1 h to burn off any volatiles and impart sufficient strength to the discs for subsequent handling and processing. A slurry of a powder mixture of 50 wt.% GDC ($Gd_{0.1}Ce_{0.9}O_{2-\delta}$ from Praxair) + 50 wt.% NiO (Atlantic Equipment Engineering) was prepared in butyl alcohol. One surface of each disc was coated with this slurry to form the anode functional layer. Slurries of GDC and YSZ were also made in butyl alcohol. The electrolyte layer was then applied on top of the anode functional layer by slurry coating. Cells with three different electrolyte variations were made. (1) GDC electrolyte layer was applied by drop coating (GDC thickness ~15 μm after sintering). (2) A thicker GDC electrolyte applied by drop coating (GDC thickness ~25 μm after sintering). (3) A tri-layer electrolyte of GDC–YSZ–GDC was formed by drop coating. The approximate thicknesses of GDC, YSZ and GDC were respectively ~12 μm, ~1 μm, and ~12 μm after sintering. After applying the electrolyte layer, the discs were sintered in air at 1450 °C for 2 h. This completed the formation of the tri-layer structure comprising the anode support–the anode functional layer–the electrolyte.

A paste of 50 wt.% GDC + 50 wt.% LSC in ethylene glycol (EG) was made. A layer of the paste was applied on the surface of the electrolyte followed by firing at 1100 °C in air for 1 h. This leads to the formation of the cathode functional layer. The final step in cell fabrication is the application of LSC current collector layer. For this step, a paste of LSC + 10 wt.% carbon was made in EG. A layer of this paste was applied on the surface of the cathode functional layer and the cell was fired at 1100 °C for 1 h in air. This completed cell fabrication.

2.3. Cell testing

Fig. 1 shows a schematic of the fixture used for cell testing. Cell test procedure used in this work is described below. A typical cell was mounted in the fixture using mica gaskets. No glass seal was used. The fixture is designed such that sealing is achieved by compression loading with load springs maintained outside the hot zone of the furnace. One silver wire mesh was pressed against the LSC current collector on the cathode side and another pressed against the anode. Two sets of silver wires were connected to the silver wire meshes for current collection and voltage measurement. The cell was heated to 600 °C while circulating 10% H_2 + balance N_2 on the anode side. The purpose of circulating H_2–N_2 gas on the anode side was to reduce Fe–Ni oxides to a Fe–Ni metallic alloy. The anode gas was subsequently changed to ~100% H_2. These steps were carried out with stagnant air on the cathode side. After 4 h, air was circulated past the cathode. Hydrogen and air flow rates were 300 and 550 ml min^{-1}, respectively. Voltage vs. current density data were collected over a temperature range between 550 °C and 650 °C.

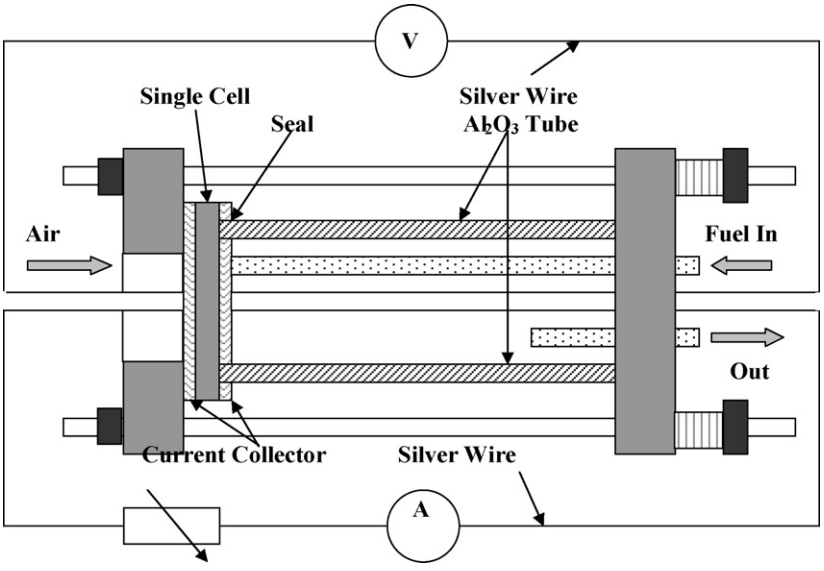

Fig. 1. A schematic of the single cell test fixture.

3. Results and discussion

3.1. Fabrication of Fe_2O_3–NiO samples and their reduction characteristics

Table 1 lists dimensional changes of samples of various compositions (Fe_2O_3 to NiO ratio) upon sintering and after subjecting sintered samples to hydrogen containing atmospheres. Shrinkage associated with sintering was between ~13% and ~19%, increasing with increasing Fe_2O_3 content. When reduced in a gas mixture containing 10% H_2 + balance nitrogen, the samples actually increased in dimensions slightly (between ~0.1% and ~0.5%) as given in Table 1. However, when reduced in 100% hydrogen atmosphere, the linear change (decrease) was greater than ~3% (or volume change of ~10%) as given Table 1. Metallic Ni is more noble compared to Fe. Thus, the oxygen partial pressure must be low enough to reduce iron oxide to metallic iron. At 800 °C, the p_{H_2}/p_{H_2O} ratio must be greater than about 1 to reduce Fe-oxides to metallic iron. Thus, presumably, the atmosphere in 10% H_2 + nitrogen mixture was not sufficiently reducing to effect the reduction of Fe–Ni-oxide samples to the metallic state, while 100% H_2 gas mixture was. Oxygen partial pressure was not measured in the fuel. Thus, it is the expectation that in 10% H_2 + balance N_2 gas, the oxygen partial pressure must have been higher, due to possible leaks in the seals.

Table 2 lists the total volume porosity of the samples after reducing in 100% H_2 at 800 °C. Note that the porosities of the samples after reduction are in excess of 50% for all compositions investigated. Typical anode-supported SOFC are made using a mixture of NiO and YSZ. Depending upon the relative amounts of NiO and YSZ and depending upon the amount of pore formers (e.g. carbon) added, porosities in the range from 30 to 50% have been reported [3,8]. It is also known that anode support porosity in excess of about 35% is generally adequate to ensure easy transport of fuel and sufficiently low concentration polarization, as long as the anode is not too thick [3]. In the present work, porosity in excess of 50% was achieved while still maintaining structural integrity. This shows that anode support made of Fe_2O_3–NiO mixtures should exhibit sufficient porosity and mechanical integrity upon reduction to function as anode support. Fig. 2 shows a scanning electron micrograph (SEM) of the anode support after reduction and testing. The SEM micrograph shows that the original grain size of the sintered oxide is on the order of a few microns. The porosity appears to be bimodal in size; coarse pores on the order of a few microns and very fine (nanometer scale to submicron) porosity within individual grains. It is anticipated that coarse pores will allow easy transport of fuel while very fine pores should provide large surface area for anode chemical reactions (such as direct internal reforming when using hydrocarbon fuels) to occur.

Table 1
Length change after sintering and reducing (10% H_2 and 100% H_2).

Composition (Fe_2O_3:NiO) (mol.%)	Length change after sintering	Length change after reducing (10% H_2)	Length change after reducing (100% H_2)
3:7	−13.4%	+0.1%	−3.6%
5:5	−16.4%	+0.2%	−3.3%
7:3	−18.9%	+0.5%	−3.2%

Table 2
Bulk density and total porosity after reducing at 800 °C with 100% H_2.

Composition (Fe_2O_3:NiO) (mol.%)	Bulk density (g cm^{-3})	Total porosity (%)
3:7	4.1	52
5:5	3.8	55
7:3	4.0	52

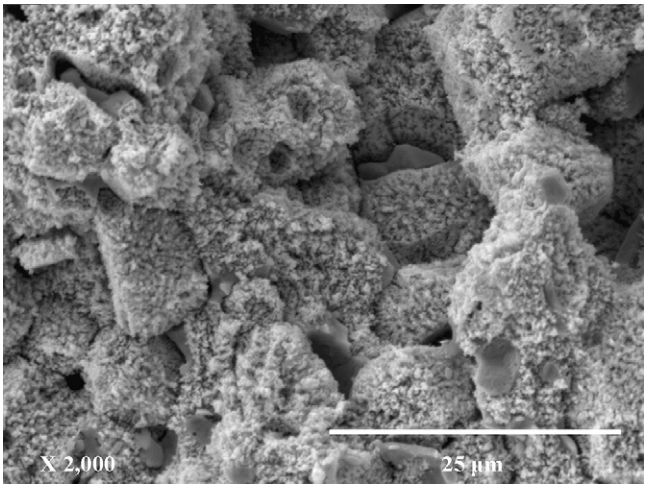

Fig. 2. An SEM micrograph of a Fe–Ni metal anode support formed by the reduction of a $NiFe_2O_4$ + NiO two-phase mixture.

Fig. 3 shows X-ray diffraction (XRD) patterns of as-sintered and reduced Fe_2O_3–NiO samples. Fig. 3(a) is an XRD pattern of as-sintered Fe_2O_3–NiO composition containing 30 mol.% Fe_2O_3 and 70 mol.% NiO. All peaks could be identified with $NiFe_2O_4$ spinel and NiO as labeled. Fig. 3(b) shows an XRD pattern after reducing. The strongest peaks in this trace correspond to an f.c.c. structure and are consistent with the presence of Fe–Ni alloys. Based on the Fe–Ni phase diagram, the anticipated phases include $FeNi_3$ and taenite (FeNi) alloy. Both are f.c.c. and with lattice parameters very close to each other. Some of the peak splitting observed in Fig. 3(b) may well also be due to the presence of Kα2 reflections. An examination of Fig. 3(b) also shows small traces of the spinel phase. It is possible that a small amount of the spinel phase may be completely

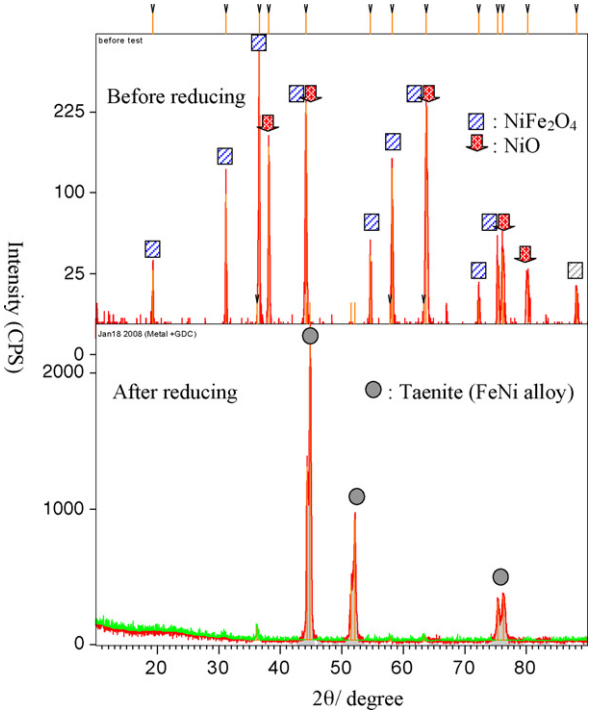

Fig. 3. XRD patterns of the as-sintered anode support and after reduction to form an alloy of Fe and Ni.

Table 3
Experimental conditions describing the three variations of the electrolyte.

Electrolyte	Details
(1) Thin GDC	GDC only, target thickness: ~15 μm
(2) Thick GDC	GDC only, target thickness: ~25 μm
(3) Tri-layer	(GDC: 12 μm) + (thin YSZ: ~1 μm) + (GDC: 12 μm)

Table 4
OCV (V) and MPD (W cm^{-2}) as a function of temperature for the three cells with three different variations of the electrolyte.

Temp.	Cond.					
	Thin GDC (~15 μm)		Thick GDC (~25 μm)		Tri-layer (GDC–thin YSZ–GDC)	
	OCV (V)	MPD (W cm^{-2})	OCV (V)	MPD (W cm^{-2})	OCV (V)	MPD (W cm^{-2})
550 °C	0.64	0.18	0.85	0.21	0.91	0.18
600 °C	0.72	0.38	0.84	0.42	0.89	0.37
650 °C	0.70	0.62	0.83	0.68	0.84	0.65

surrounded by the metallic phase formed thereby preventing its access to the reducing atmosphere (Tables 3 and 4).

3.2. Microstructure of single cells

Fig. 4 shows an SEM micrograph of the fractured surface of a typical cell after testing. The thicknesses of the various layers are as follows: (1) anode layer: ~0.9 mm; (2) anode interlayer (or functional layer): ~20 μm; (3) GDC electrolyte: ~25 μm; (4) cathode interlayer (or functional layer): ~15 μm; (5) cathode current collector: ~40 μm. The GDC electrolyte is essentially fully dense with no open porosity. The anode functional and cathode functional layers are porous with fine microstructures. The anode support is porous of a coarse microstructure with bimodal porosity – large pore size in between particles and very fine porosity within individual particles (same as in Fig. 2). Fig. 5 shows an SEM micrograph of a cell with EDX line scan superimposed on the micrograph. The figure shows Ce, Fe and Ni traces. No Ni or Fe was detected in the GDC electrolyte. The presence of Ni and Fe was seen in the anode support and no Ce was detected. In the anode functional layer, all three elements were detected consistent with the initial formulation of the anode functional layer and interdiffusion of Fe and Ni.

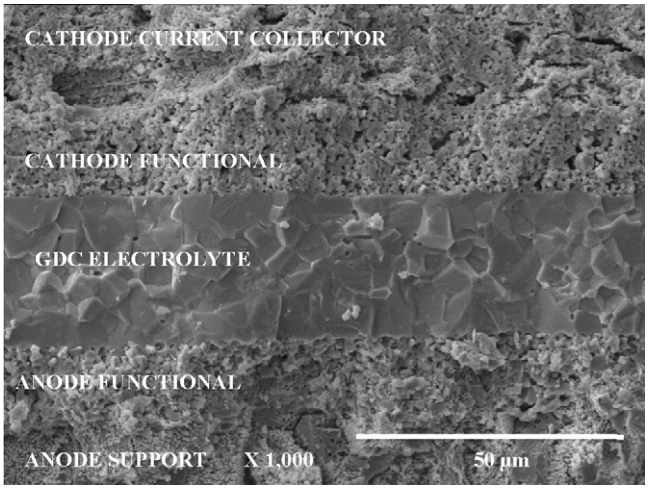

Fig. 4. SEM micrograph of a typical tested cell.

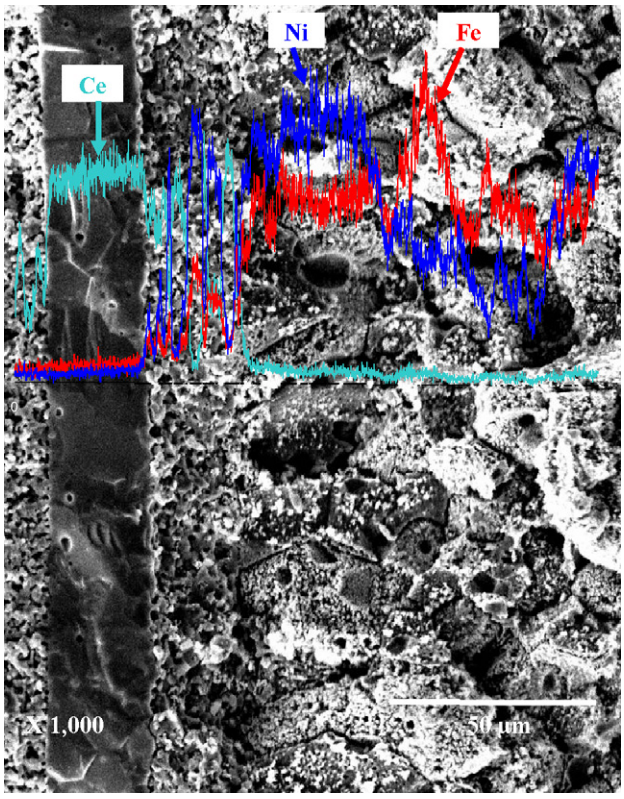

Fig. 5. An EDX line scan across a tested cell.

3.3. Single cell test results

Figs. 6–8 show the performance curves for three different cells with three different variations of the electrolyte. Fig. 6 is for the cell with GDC electrolyte of ~25 μm in thickness. The tests were performed at three temperatures: 550 °C, 600 °C, and 650 °C. The open circuit voltage was between ~0.83 V and ~0.85 V. The maximum power density ranged between ~0.2 W cm^{-2} at 550 °C and ~0.68 W cm^{-2} at 650 °C. The voltage vs. current density plots are convex up. Typically cells made with YSZ as the electrolyte exhibit voltage vs. current density plots that are concave up at low current densities. The observed convex up curvature has been attributed to the mixed ionic electronic conducting properties of ceria [9]. Fig. 7 shows performance curves for a cell with GDC electrolyte thick-

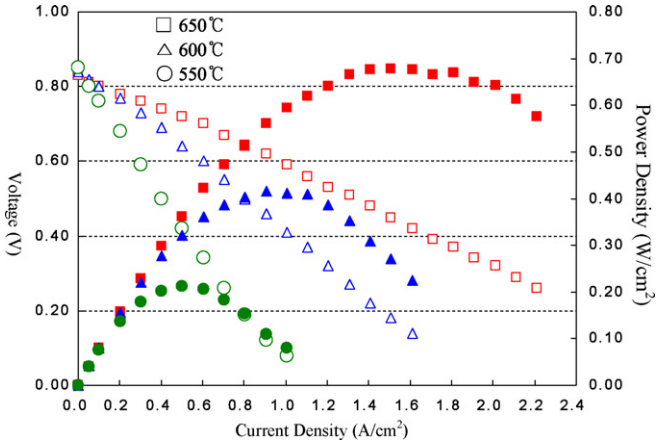

Fig. 6. Voltage and power density vs. current density plots at 550 °C, 600 °C and 650 °C for a cell with a GDC electrolyte ~25 μm thick.

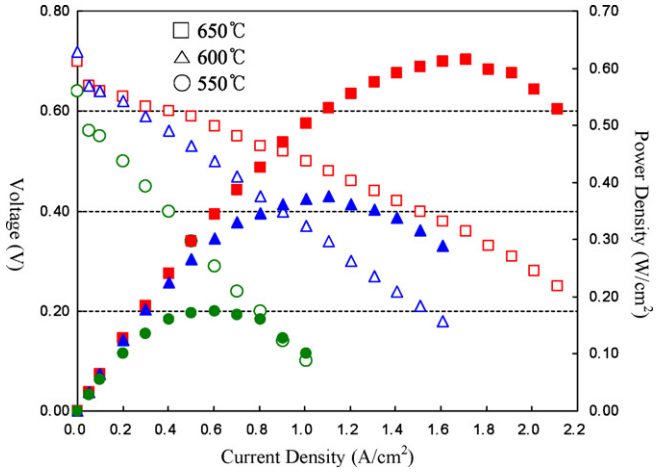

Fig. 7. Voltage and power density vs. current density plots at 550 °C, 600 °C and 650 °C for a cell with GDC electrolyte ~15 μm thick.

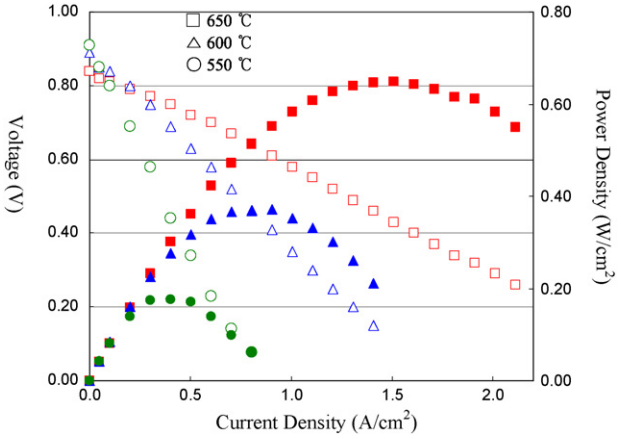

Fig. 8. Voltage and power density vs. current density plots for a tri-layer electrolyte cell at 550 °C, 600 °C, and 650 °C.

ness of ~15 μm. The OCV of the cell was much lower. This behavior has been observed [10–12] and has been attributed to the overall lower ionic transport number for the thinner membranes [13–15]. The maximum power density ranged between ~0.18 W cm^{-2} at 550 °C and ~0.62 W cm^{-2} at 650 °C. Slightly lower performance even with a thinner electrolyte is thus attributed to lower OCV. This suggests that a somewhat thicker electrolyte is preferred. Fig. 8 shows voltage vs. current density performance curves for a cell with GDC/YSZ/GDC tri-layer electrolyte of ~25 μm in thickness. A slightly higher OCV was observed indicating that the ~1 μm YSZ layer probably did not completely dissolve in GDC during the sintering process and was effective in partially blocking the electronic current. The maximum power density, however, was less than a cell with ~25 μm GDC electrolyte. Further work is needed to improve processing and determine if the electronic current can be blocked off without significantly increasing the ohmic contribution.

4. Summary

Anode-supported cells with Gd_2O_3-doped ceria as electrolyte and anode support comprising a mixture of Fe and Ni were fabricated and their performance was measured over a range of temperatures between 550 °C and 650 °C with hydrogen as fuel and air as oxidant. The anode support precursor consisted of Fe_2O_3 and NiO in 3 to 7 ratio (Fe to Ni ratio 6 to 7) on a molar basis. The anode functional layer was a mixture of Ni and GDC, and the cathode functional layer was a mixture of Sr-doped $LaCoO_3$ (LSC) and GDC. In the as-sintered state, the anode support contained predominantly $NiFe_2O_4$ spinel with some NiO. Upon reduction in a hydrogen-containing atmosphere, $NiFe_2O_4$ and NiO were reduced to form a porous metallic alloy of Fe and Ni. The porosity was adequate to function as anode support. Maximum power density as high as ~0.68 W cm^{-2} was measured at 650 °C. The present results show that Fe–Ni metal anode-supported cells with GDC electrolyte can be successfully fabricated and exhibit good performance.

Acknowledgements

This work was supported by the U.S. Department of Energy under Grant Number DE-FG02-06ER46086. Dr. Feng Zhao is acknowledged for experimental assistance in the early stages of the work.

References

[1] M.C. Williams, J. Strakey, W. Surdoval, J. Power Sources 159 (2006) 1241–1247.
[2] S.C. Singhal, K. Kendall, High Temperature Solid Oxide Fuel Cell, Elsevier, 2004.
[3] F. Zhao, A.V. Virkar, J. Power Sources 141 (2005) 79–95.
[4] P. Bance, N.P. Brandon, B. Girvan, P. Holbeche, S. O'Dea, B.C.H. Steele, J. Power Sources 131 (2004) 86–90.
[5] M.C. Tucker, G.Y. Lau, C.P. Jacobson, L.C. DeJonghe, S.J. Visco, J. Power Sources 175 (2008) 447–451.
[6] J. Yan, M. Enoki, H. Matsumoto, T. Ishihara, Electrochem. Solid-State Lett. 10 (9) (2007) B139–B141.
[7] J.L. Murray, L.H. Bennett, H. Baker, T.B. Massalski, Binary Alloy Phase Diagrams ASM 1 (1986) 1086.
[8] J.W. Kim, A.V. Virkar, K.-Z. Fung, K. Metha, S.C. Singhal, J. Electrochem. Soc. 146 (1) (1999) 69–78.
[9] I. Reiss, M. Godckemeier, L.J. Gauckler, Solid State Ionics 90 (1996) 91–104.
[10] J.H. Joo, K.M. Choi, Solid State Ionics 178 (2007) 1602–1607.
[11] T. Matsui, T. Kosaka, M. Inaba, A. Mineshige, Z. Ogumi, Solid State Ionics 176 (2005) 663.
[12] H.T. Lim, A.V. Virkar, J. Power Sources 180 (2008) 92–102.
[13] M.H. Hebb, J. Chem. Phys. 20 (1952) 185.
[14] L. Heyne, Mass Transport in Oxides, vol. 296, NBS Special Publication, 1968, p. 149.
[15] C. Wagner, Prog. Solid-State Chem. 10 (1) (1975) 3–16.